CHEMISTRY
AN ASIAN JOURNAL

DOI: 10.1002/asia.201100879

Multifunctional Core–Shell Upconverting Nanoparticles for Imaging and Photodynamic Therapy of Liver Cancer Cells

Zengxia Zhao,[a] Yuning Han,[a] Chenghong Lin,[b] Dong Hu,[a] Fang Wang,[a] Xiaolan Chen,*[a] Zhong Chen,[b] and Nanfeng Zheng*[a]

Abstract: Lanthanide-doped upconversion nanoparticles (UCNPs) have attracted considerable attention for their application in biomedicine. Here, silica-coated $NaGdF_4$:Yb,Er/$NaGdF_4$ nanoparticles with a tetrasubstituted carboxy aluminum phthalocyanine (AlC_4Pc) photosensitizer covalently incorporated inside the silica shells were prepared and applied in the photodynamic therapy (PDT) and magnetic resonance imaging (MRI) of cancer cells. These UCNP@SiO_2(AlC_4Pc) nanoparticles were uniform in size, stable against photosensitizer leaching, and highly efficient in photogenerating cytotoxic singlet oxygen under near-infrared (NIR) light. In vitro studies indicated that these nanoparticles could effectively kill cancer cells upon NIR irradiation. Moreover, the nanoparticles also demonstrated good MR contrast, both in aqueous solution and inside cells. This is the first time that $NaGdF_4$:Yb,Er/$NaGdF_4$ upconversion-nanocrystal-based multifunctional nanomaterials have been synthesized and applied in PDT. Our results show that these multifunctional nanoparticles are very promising for applications in versatile imaging diagnosis and as a therapy tool in biomedical engineering.

Keywords: cancer · lanthanides · magnetic resonance imaging · nanoparticles · photodynamic therapy

Introduction

Photodynamic therapy (PDT) is a promising technique for the treatment of various types of cancer.[1–4] In this technique, photosensitizers (PSs) are brought into or onto the corresponding cancer tissue and irradiated with a laser. Upon irradiation, the activated PSs transfer energy to ground-state oxygen molecules to generate cytotoxic singlet oxygen ($^1O_2$) that can irreversibly damage the diseased cells and tissues.[5,6] For an effective and efficient PDT, the judicious selection of PS is crucial. To date, several types of PSs, such as porphyrin derivatives, chlorins, and phthalocyanines, have been developed and used in the clinical treatment of certain cancers.[7–9] However, most of these aforementioned PSs are excited by visible light, which only penetrates tissue a few millimeters in depth, and so they are usually only suitable for treating epithelial tumors, such as skin or breast tumors, and are less effective for internal or large tumors.[10] In biological tissues, the good optical transmission window is in the near-infrared (NIR) range (700–1000 nm),[11] which affords deep light penetration, low autofluorescence and photodamage, and reduced light scattering. Therefore, for practical applications, the exploration of new PSs that can be activated with NIR light is of particular interest. Herein, we used 980 nm laser beam to irradiate α-$NaGdF_4$:Yb,Er/$NaGdF_4$ upconversion nanocrystals and then utilized the emission from the nanocrystal to activate a tetrasubstituted carboxy aluminum phthalocyanine PS for the photodynamic therapy of liver cancer cells.

The use of biocompatible carriers, such as microcapsules, liposomes, oligopeptides, polymeric micelles, and upconversion-nanocrystal-decorated nanosystems, to deliver PSs have been reported to improve PDT efficiency.[12–27] These drug carriers not only enhance the reactivity of PSs, but can also be tailored to an appropriate size for their preferential accumulation at the tumor site owing to a phenomenon known as the "enhanced permeability and retention effect".[22] Among these various delivery platforms, nanoparticle systems containing lanthanide-doped NIR-to-visible upconversion nanoparticles (UCNPs) have gained significant recent attention.[23–27] For instance, silica-coated $NaYF_4$ ($NaYF_4$@silica) upconversion nanoparticles, which have the photosensitizer merocyanine 540 incorporated into the silica shells, were synthesized and used in PDT by Zhang et al.[23] Mesoporous-silica-coated $NaYF_4$@silica nanoparticles with core/shell structures were also reported for synergistic optical imaging and PDT applications.[25] In comparison with

[a] Z. Zhao, Y. Han, D. Hu, F. Wang, Prof. X. Chen, Prof. N. Zheng
State Key Laboratory for Physical Chemistry of Solid Surfaces and the Department of Chemistry
College of Chemistry and Chemical Engineering
Xiamen University
Xiamen, 361005 (P.R. China)
Fax: (+86) 592-2183047
E-mail: chenxl@xmu.edu.cn
nfzheng@xmu.edu.cn

[b] C. Lin, Prof. Z. Chen
Departments of Electronic Science and Communication Engineering
Fujian Key Laboratory of Plasma and Magnetic Resonance
Xiamen University
Xiamen, 361005 (P.R. China)

Supporting information for this article is available on the WWW under http://dx.doi.org/10.1002/asia.201100879.

other PDT carrier systems, UCNP-based carriers have the following prominent advantages: 1) they can be excited with NIR radiation, which penetrates biological tissue as deep as several centimeters without damaging the tissue; 2) they can emit at various wavelengths (blue, green, red, etc.) by an appropriate choice of the doping emitter ions; 3) the strong UV/Vis emissions can be further absorbed by the adjacent PS molecules to generate $^1O_2$ to kill cancer cells; and 4) these systems can be developed with multifunctional capabilities for simultaneous imaging (fluorescence or magnetic resonance) diagnosis and PDT therapy by changing the type of UCNPs. Previously reported upconversion nanocrystals for PDT were mainly based on $NaYF_4$ UCNPs.[23–27] To the best of our knowledge, the application of $NaGdF_4$ UCNPs in PDT has not yet been reported. Moreover, PSs are typically loaded into such $NaYF_4$-based composite nanoparticles through noncovalent interactions, which can cause leaking problems in harsh biological environments.

Herein, we report the synthesis of $NaGdF_4$:Yb,Er/$NaGdF_4$ core, PS-doped silica shell nanocomposites, and their applications in the magnetic resonance imaging (MRI) and PDT of cancer cells. A new PS, tetrasubstituted carboxy aluminum phthalocyanine (AlC_4Pc; see the Supporting Information, Figure S1), was covalently linked to the silica shells during the silica-coating process. Under NIR-light excitation (980 nm), the upconversion luminescence from Er^{3+} doped in the $NaGdF_4$ UCNPs (650–670 nm) was used to activate photosensitizing molecules of AlC_4Pc, which had strong absorbance in the same spectral region as the red emission of the UCNPs, and to generate cytotoxic $^1O_2$ to kill cancer cells. Gd^{3+} ions in the host matrix imparted short t_1 (spin-lattice relaxation time) and t_2 (spin–spin relaxation time), which facilitated high-contrast MR imaging. Compared with previously reported silica- or mesoporous-silica-coated UCNP photosensitizer carriers,[23,25] our $NaGdF_4$-based nanocomposite had a small size-controllable diameter (ca. 38 nm), which improved cell-uptake efficiency owing to the size-dependent uptake of cells on the particles.[28,29] The thin, biocompatible silica shell also ensured that the UCNP and PSs were in close proximity to one another, which maximized the photosensitizer excitation efficiency. Moreover, the covalent coupling of PSs in the rigid network structure helped to obviate the degradation of PS in harsh biological environments, and to overcome their premature release. We demonstrated the effectiveness of these nanocomposites in PDT and MRI by in vitro cell experiments. This is the first report of the application of $NaGdF_4$-based nanocomposites in both MRI and PDT.

Abstract in Chinese:

稀土上转换纳米晶在生物医学中的应用引起了研究者的浓厚兴趣。本文制备了二氧化硅包覆的 α-$NaGdF_4$: Yb^{3+}, Er^{3+} / $NaGdF_4$ *上转换复合纳米颗粒*（UCNP@SiO_2(AlC_4Pc)），在这些复合纳米颗粒中光敏剂四羧基铝酞菁共价结合在硅壳内。这些 UCNP@SiO_2(AlC_4Pc)纳米颗粒尺寸均一可控，光敏剂不易泄漏，在近红外光激发下具有高效的单线态氧产生能力。体外研究表明：这些复合纳米颗粒在近红外光辐射下能有效杀死癌细胞。此外，这些纳米颗粒在水溶液和细胞内均具有良好的磁共振对比效果。该研究首次报道了基于 $NaGdF_4$: Yb^{3+}, Er^{3+}的多功能纳米颗粒在光动力学治疗中的应用。这些纳米颗粒有望作为多功能的诊断和治疗工具用于生物医学工程研究。

Results and Discussion

Synthesis and Characterization of UCNP@SiO_2(AlC_4Pc) Nanoparticles

Upconversion $NaGdF_4$:Yb,Er/$NaGdF_4$ (UCNPs) nanocrystals were prepared by thermal decomposition, according to a literature procedure.[30] TEM analysis showed that the UCNPs were uniform in size with an edge-length of about 22 nm (Figure 1 a). The crystalline phase of the UCNPs was further characterized using high-resolution TEM (HRTEM) and X-ray diffraction (XRD) analysis. HRTEM of a single UCNP nanoparticle indicated that the distance between lattice fringes was 0.277 nm (Figure 1 a, inset), which corresponded to the *d* spacing for the (200) lattice plane in the cubic $NaGdF_4$ structure. As shown in Figure 1 c, the peak positions agreed well with the standard PDF data of cubic α-$NaGdF_4$ (JCPDS No. 27-0697).[31] This result indicated that high-purity $NaGdF_4$:Yb,Er/$NaGdF_4$ nanocrystals were obtained with good crystallinity, which is very beneficial for obtaining bright luminescence. The as-prepared UCNPs were then coated with a layer of silica to form UCNP@SiO_2 nanoparticles by using a reverse-micelle method. To covalently bind the photosensitizer molecules (AlC_4Pc) into the silica layer, AlC_4Pc was treated with APTES in advance to form an APTES-AlC_4Pc conjugate. The conjugate was then co-hydrolyzed with TEOS to form a thin silica coating on the upconversion nanocrystals. The as-prepared AlC_4Pc-doped UCNP@SiO_2 nanoparticles (UCNP@SiO_2(AlC_4Pc)) were highly uniform in size, about 38 nm in diameter (Fig-

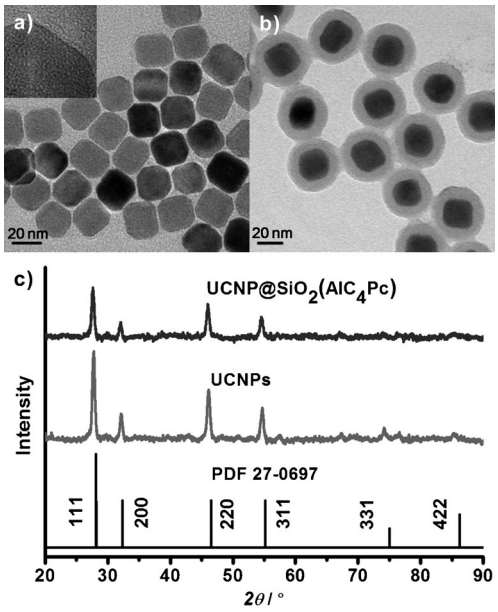

Figure 1. TEM images of a) as-prepared $NaGdF_4$:Yb,Er/$NaGdF_4$ nanocrystals (UCNPs) and b) UCNP@SiO_2(AlC_4Pc) nanoparticles; inset: high-resolution TEM image. c) XRD patterns of UCNPs, UCNP@SiO_2(AlC_4Pc) nanoparticles, and standard patterns of pure cubic-phase $NaGdF_4$ (JCPDS No. 27-0697).

ure 1b) and were easily dispersed in water. The thickness of the silica shell was easily regulated from 3–10 nm by varying the amount of TEOS (see the Supporting Information, Figure S2), which allowed us to effectively control the diameter of the UCNP@SiO_2(AlC_4Pc) nanoparticles in the range of 28–42 nm. We chose particles with diameters of about 38 nm for our following experiments. Successful silica coating was further confirmed by energy-dispersive X-ray analysis (EDXA; see the Supporting Information, Figure S3) and by XRD analysis (Figure 1c). EDXA analysis showed the presence of Si, Gd, F, Yb, and Er in the sample of UCNP@SiO_2(AlC_4Pc) nanoparticles, whilst there was no signal for Si in the sample of parent UCNPs. Moreover, the peaks in the XRD pattern of UCNP@SiO_2(AlC_4Pc) (Figure 1c) were consistent with that of pure cubic-phase $NaGdF_4$ crystals; however, the intensity was weak, owing to the influence of amorphous SiO_2.

The UCNP@SiO_2(AlC_4Pc) nanoparticles formed a clear-blue solution in PBS buffer (phosphate-buffered saline; Figure 2a, inset). Dynamic light scattering (DLS) measurements showed a sharp peak at around 50 nm, thereby indicating that the UCNP@SiO_2(AlC_4Pc) nanoparticles had good dispersibility in water (Figure 2a). UV/Vis spectra of the UCNP@SiO_2(AlC_4Pc) nanoparticles showed that the nanoparticles displayed similar absorption features to free AlC_4Pc, with a Q-band at about 685 nm (Figure 2b), thus implying that the structure of AlC_4Pc molecules in the nanoparticles was well-retained. According to the calibration curve of the UV/Vis absorption spectra of free AlC_4Pc, the AlC_4Pc content in the UCNP@SiO_2(AlC_4Pc) nanoparticles was around 3.3 wt%.

The entrapment efficiency (AlC_4Pc incorporated into the nanoparticles/total initial $AlC_4Pc \times 100\%$) of AlC_4Pc in the UCNP@SiO_2(AlC_4Pc) nanoparticles was determined by UV/Vis absorption spectra to be approximately 100%. Because AlC_4Pc was covalently linked to the silica matrix, we expected that the leakage of AlC_4Pc from the nanoparticles could be avoided. The release of AlC_4Pc from the UCNP@SiO_2(AlC_4Pc) nanoparticles was also investigated in PBS solution (pH 7.40) and in a DMEM cell culture medium. Sample solutions were taken every 24 hours and centrifuged. The supernatants were then subjected to UV/Vis absorption measurements. The results showed no leakage of AlC_4Pc from UCNP@SiO_2(AlC_4Pc) nanoparticles incubated in the two solutions for up to 5 days (Figure 2d), thereby suggesting that these nanoparticles were very stable against PS leaching. The good stability of these nanoparticles makes them good candidates for various biological applications.

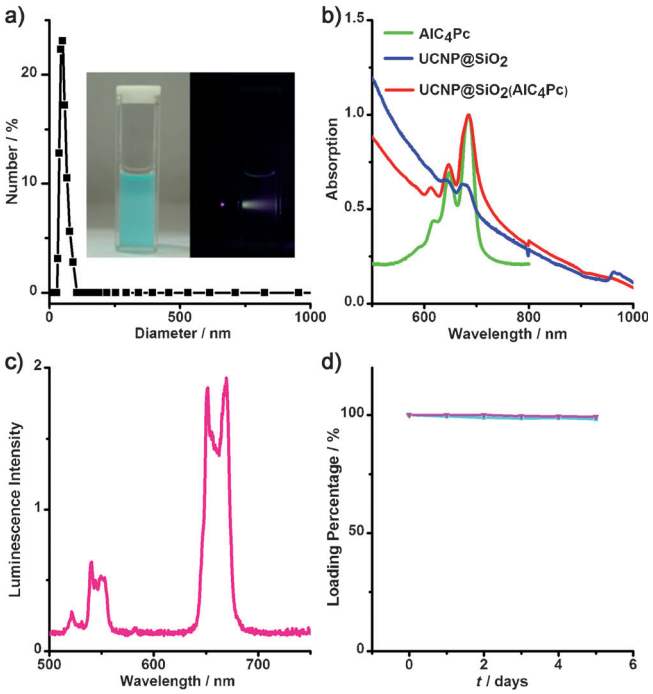

Figure 2. a) Size distribution of UCNP@SiO_2(AlC_4Pc) nanoparticles in water; inset: photographs of UCNP@SiO_2(AlC_4Pc) nanoparticles in PBS under ambient light and 980 nm laser excitation. b) UV/Vis absorption spectra of AlC_4Pc, UCNP@SiO_2, and UCNP@SiO_2 (AlC_4Pc) in PBS buffer (pH 7.40). c) Emission spectra of UCNP@SiO_2 nanoparticles upon excitation with a 980 nm laser. d) The release of AlC_4Pc from the UCNP@SiO_2(AlC_4Pc) nanoparticles in PBS (blue line) and in the cell medium (pink line).

Luminescence Properties and Singlet-Oxygen Detection of UCNP@SiO_2(AlC_4Pc) Nanoparticles

As shown in Figure 2c, under the excitation of a 980 nm NIR laser, the UCNP@SiO_2 nanoparticles showed multiple characteristic Er^{3+} emission peaks at 521, 540, and 549 nm (green bands) and 651, 654, and 669 nm (red bands). The green bands were attributed to transitions from the $^2H_{11/2}$ and $^4S_{3/2}$ excited states of the Er^{3+} ions to the $^4I_{15/2}$ ground state, whereas the red bands corresponded to transitions from the $^4F_{9/2}$ excited state to the $^4I_{15/2}$ ground state. As shown in Figure 2b, the cubic α-phase UCNP@SiO_2 nanoparticles displayed intense red emission and considerable overlay with the Q-band absorption of doped AlC_4Pc. This overlap ensured that AlC_4Pc could effectively absorb the emitted luminescent radiation of UCNP@SiO_2 nanoparticles and be activated to produce reactive oxygen species when the nanoparticles were excited with a 980 nm laser.

Singlet oxygen is thought to be the major cytotoxic species that causes cell death through the so-called type II mechanism.[32] As a potential second-generation photosensitizer, AlC_4Pc exhibits high efficiency of singlet-oxygen photogeneration.[20] In this study, the $^1O_2$-generation capability of the UCNP@SiO_2(AlC_4Pc) nanoparticles was assessed using 1,3-diphenylisobenzofuran (DPBF), a singlet-oxygen chemical probe, in CH_3CN, under 980 nm laser irradiation (500 mW cm^{-2}).[33] DPBF reacts irreversibly with $^1O_2$ and the reaction can be followed by recording the decrease in the intensity of the DPBF absorption at around 400 nm. The changes in the absorption spectra of DPBF in the presence of UCNP@SiO_2(AlC_4Pc) nanoparticles after different irradiation times are shown in Figure 3. Control tests were carried out to confirm that the decrease in the absorption of DPBF

CHEMISTRY
AN ASIAN JOURNAL

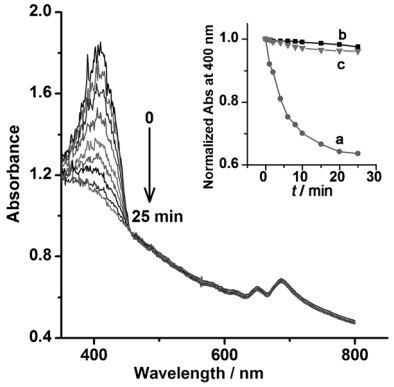

Figure 3. Absorption spectra of UCNP@SiO_2(AlC_4Pc) nanoparticles in the presence of DPBF after different irradiation times with a 980 nm laser beam; inset: decay curves of the absorption of DPBF as a function of irradiation time. a) DPBF with UCNP@SiO_2(AlC_4Pc) nanoparticles, b) DPBF with UCNP@SiO_2 nanoparticles, and c) DPBF with free AlC_4Pc in CH_3CN.

was induced by singlet oxygen (Figure 3, inset). In the presence of UCNP@SiO_2(AlC_4Pc) nanoparticles, the DPBF absorption at 400 nm dramatically decreased under NIR-laser irradiation (Figure 3, curve a, inset), thereby suggesting that these nanoparticles were highly efficient in the generation of reactive $^1O_2$. In contrast, there were no obvious decreases in DPBF absorbance for solutions containing UCNP@SiO_2 nanoparticles (Figure 3, curve b) or free AlC_4Pc (Figure 3, curve c). The effective $^1O_2$-generating capability of our nanoparticles under NIR light made it possible for them to be applied in NIR-induced PDT.

It is interesting to note that there was no obvious change in the absorption in the range 600–700 nm (which is mainly due to AlC_4Pc molecules), thus suggesting that the AlC_4Pc molecules were not affected during the radiation. This result was consistent with previous reports that suggested that a covalently linked structure between the PS and silica would increase photosensitizer stability.[34]

NIR-Induced In Vitro PDT on Mouse Liver Cancer Cells

Before the in vitro PDT studies in cells were performed, the cytotoxicity of the UCNP@SiO_2(AlC_4Pc) nanoparticles on BNL 1 ME A. 7R.1 cells (abbreviated as MEAR cells) were evaluated by using the standard MTT assay. The viability of untreated cells was assumed to be 100%. As displayed in Figure 4a, the UCNP@SiO_2(AlC_4Pc) nanoparticles showed very low cytotoxicity toward MEAR cells at relatively low concentrations ($\leqq 50\ \mu g\,mL^{-1}$). When the concentration of UCNP@SiO_2(AlC_4Pc) nanoparticles increased to $500\ \mu g\,mL^{-1}$, the cell viability remained above 60%. Furthermore, from the cell morphology (Figure 4b), the MEAR cells were found to retain good biological activity after incubation with nanoparticles at a concentration of $100\ \mu g\,mL^{-1}$ for 24 hours. These results indicated that UCNP@SiO_2 (AlC_4Pc) nanoparticles had good biocompatibility.

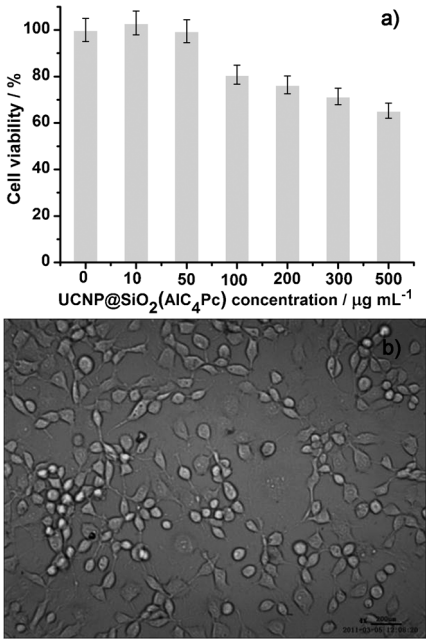

Figure 4. a) The viability of MEAR cells incubated with UCNP@SiO_2 (AlC_4Pc) nanoparticles at different concentrations, (±5)% of standard deviation. b) The cell morphology of MEAR cells incubated with UCNP@SiO_2(AlC_4Pc) nanoparticles at $100\ \mu g\,mL^{-1}$ for 24 h.

The cellular uptake of the UCNP@SiO_2(AlC_4Pc) nanoparticles was also confirmed by both confocal microscopy and ICP-AES (for gadolinium content). As shown in Figure 5, after 12 hours incubation with MEAR cells, red fluorescence from the nanoparticles was observed in the cells and the nanoparticles were mainly located at the cytoplasmic regions, whereas the control cells incubated without the nanoparticles showed no fluorescence under similar imaging parameters and conditions (data not shown). The efficiency of the nanoparticle uptake by MEAR cells was evaluated by incubating the cells with different concentrations of the nanoparticles for 24 hours. We observed that the accumulation of nanoparticles increased in the cells with an increasing concentration of nanoparticles (see the Supporting Information, Figure S4). These results indicated that the UCNP@SiO_2(AlC_4Pc) nanoparticles had good endocytosis capability and could be used for both imaging and therapy. Taking both these cytotoxicity and uptake results into consideration, we chose $100\ \mu g\,mL^{-1}$ as the optimal concentration of nanoparticles for use in the photocytotoxic experiments.

Next, we studied the effectiveness of the UCNP@SiO_2 (AlC_4Pc) nanoparticles in the destruction of cancer cells triggered by NIR light. After 12 hours of incubation with these nanoparticles ($100\ \mu g\,mL^{-1}$), the MEAR cells were irradiated with a 980 nm laser ($0.5\ W/cm^2$) for 2 or 5 minutes. The dead cells were then stained with trypan blue, a vitality dye that only stains cells where the membrane is damaged. Microscopic images of MEAR cells after different treatments are shown in Figure 6. Significant cell death was observed for MEAR cells incubated with UCNP@SiO_2

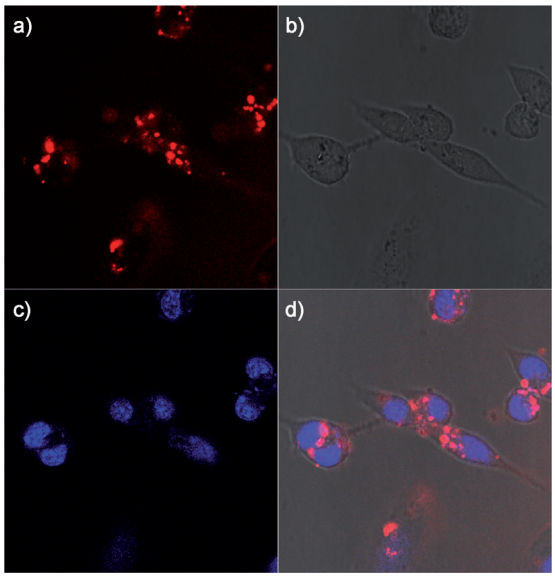

Figure 5. Confocal fluorescence images of MEAR cells after incubation with UCNP@SiO_2(AlC_4Pc) nanoparticles for 12 h. The cell nuclei were stained with DAPI (blue fluorescence). a) nanoparticle fluorescence, b) bright-field, and c) DAPI fluorescence images, d) merging of images (a–c).

(AlC_4Pc) nanoparticles after exposure to the 980 nm laser: nearly 40% cells were killed after 5 minutes of irradiation (Figure 6b). Using NIR irradiation alone did not cause obvious cell damage (Figure 6c); cells incubated with UCNP@SiO_2 nanoparticles (Figure 6d) or free AlC_4Pc alone (Figure 6e) also showed no obvious cell death under the same NIR-light exposure. From these results, we concluded that the absorption peak of AlC_4Pc at approximately 685 nm overlapped with the red emission peak of the upconversion $NaGdF_4$:Yb,Er/$NaGdF_4$ nanocrystals. Thus, the light emitted by the nanocrystals activated AlC_4Pc to release singlet oxygen species to kill the surrounding cancer cells.

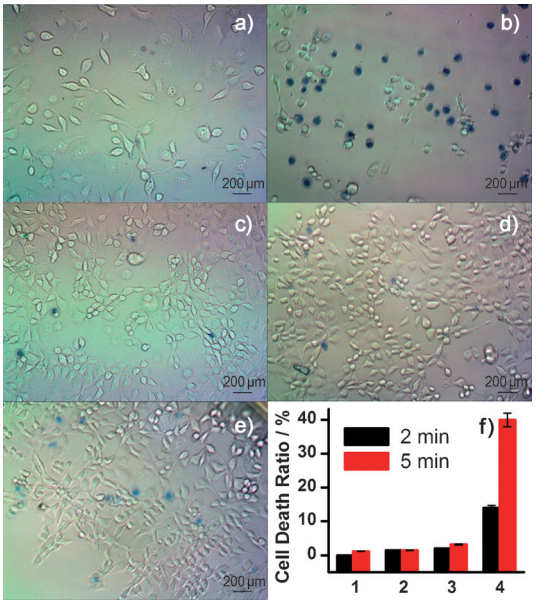

Figure 6. Optical imaging of MEAR cells stained with trypan blue after treatment a) without nanoparticles and without light exposure; b) with 100 μg mL^{-1} UCNP@SiO_2(AlC_4Pc) nanoparticles and 5 min NIR light exposure; c) without nanoparticles and 5 min NIR light exposure; d) with 100 μg mL^{-1} UCNP@SiO_2 nanoparticles and 5 min NIR light exposure; e) with free AlC_4Pc (4.44×10^{-6} mol L^{-1}) and 5 min NIR light exposure; f) comparison of cell death ratios after different treatments: 1) only cells, 2) cells+UCNP@SiO_2, 3) cells+free AlC_4Pc, 4) cells+UCNP@SiO_2(AlC_4Pc) nanoparticles. Black column: 2 min NIR-light exposure, orange column: 5 min NIR-light exposure.

Magnetic Resonance Imaging of Cancer Cells

Many lanthanide ions exhibit remarkable paramagnetic properties and have been used in MRI as contrast agents.[35] In our study, the paramagnetic behavior of the Gd^{3+}-doped fluoride nanocrystals and their use as contrast agents were also examined. The MR relaxivities of the UCNP@SiO_2(AlC_4Pc) nanoparticles dispersed in water are shown in Figure 7a. The longitudinal (r_1) and transverse relaxivities (r_2) were 1.24 mM^{-1} s^{-1} and 31.13 mM^{-1} s^{-1} on a per-millimolar Gd^{3+} basis, respectively. The MR relativity data were comparable with other reported Gd-based UCNP contrast agents.[30,35,36] Representative t_1-weighted and t_2-weighted images of aqueous nanoparticle solutions with different concentrations are shown in Figure 7b. The signal clearly increased with the concentration of the nanoparticles under the t_1-weighted mode, whilst the signal gradually darkened with an increase in the nanoparticle concentration under the t_2-weighted mode. These results suggested that the nanoparticles could be used for both t_1- and t_2-weighted MR imaging. We also examined the t_2-weighted MR-contrast effect of the UCNP@SiO_2(AlC_4Pc) nanoparticles inside the cells. As shown in Figure 7c, the brightness of cells clearly darkened with increasing nanoparticle concentration, owing to the decrease in t_2 relaxation.

Conclusions

We have developed a facile strategy to synthesize core–shell upconversion nanoparticles with precise size-control and good dispersities. α-$NaGdF_4$:Yb,Er/$NaGdF_4$ (UCNP) nanocrystals encapsulated inside the silica shell converted NIR light to strong red-light emission, which was captured by photosensitizer molecules (AlC_4Pc) covalently linked to the silica shell. These UCNP@SiO_2(AlC_4Pc) nanoparticles exhibited good stability against leaching and excellent efficiency in photogenerating cytotoxic singlet oxygen upon excitation by a NIR laser, which allowed a deeper light penetration depth than visible-light excitation. In vitro studies indicated that the UCNP@SiO_2(AlC_4Pc) nanoparticles can enter cancer cells and effectively kill cancer cells after being exposed to NIR light. Moreover, the good t_1 and t_2 relaxivity capabilities of UCNPs were demonstrated in cell MRI imaging. Our study has possible applications in future imaging-guided therapy studies.

CHEMISTRY
AN ASIAN JOURNAL

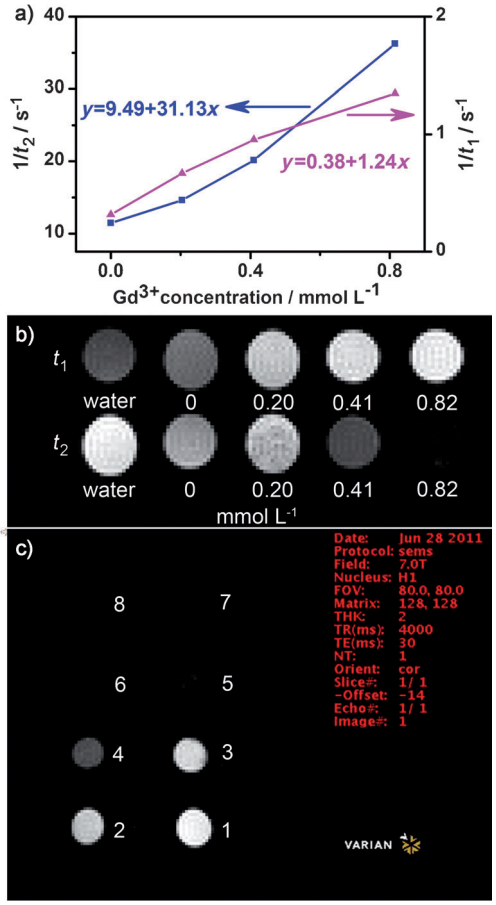

Figure 7. a) Longitudinal (r_1) and transverse (r_2) relaxivities of UCNP@SiO_2(AlC_4Pc) nanoparticles. b) t_1-weighted (TR 100 ms, TE 15 ms) and t_2-weighted MR images (TR 4000 ms, TE 50 ms) of aqueous UCNP@SiO_2(AlC_4Pc) nanoparticles (0 represents pure SiO_2 nanoparticles). c) t_2-weighted MRI of MEAR cells incubated with UCNP@SiO_2(AlC_4Pc) nanoparticles at various concentrations for 12 h: 1) cell medium; 2) pure SiO_2 nanoparticles; UCNP@SiO_2(AlC_4Pc) at 3) 0.10, 4) 0.20, 5) 0.41, 6) 0.82, 7) 1.20, and 8) 1.60 mmol L^{-1} of Gd^{3+} ions. The corresponding UCNP@SiO_2(AlC_4Pc) nanoparticle concentrations were: 3) 45, 4) 90, 5) 185, 6) 369, 7) 540 and 8) 720 μg mL^{-1}, respectively. The amount of Gd^{3+} ions in the UCNP@SiO_2(AlC_4Pc) nanoparticles were determined by the ICP-AES method. The relaxivities were determined at room temperature (25 °C) and at 300 MHz.

Experimental Section

Materials

Gadolinium oxide (Gd_2O_3, 99.99 %), ytterbium oxide (Yb_2O_3, 99.99 %), erbium oxide (Er_2O_3, 99.99 %), trifluoroacetic acid (CF_3COOH, 99 %), sodium trifluoroacetate (CF_3COONa, 98 %), Igepal CO-520, tetraethoxysilane (TEOS), 3-aminopropyltriethoxysilane (APTES), ethyl-[3-(dimethylamino)propyl]-carbodiimide hydrochloride (EDC), *N*-hydroxysuccinimide (NHS), 3-[4,5-dimethylthiazol-2-yl]-2,5-diphenyltetrazolium bromide (MTT), and 1,3-diphenylisobenzofuran (DPBF) were purchased from Sigma-Aldrich. Oleic acid (technical grade, 90 %) and 1-octadecene (technical grade, 90 %) were purchased from Alfa Aesar. Tetrasubstituted carboxy aluminum phthalocyanine (AlC_4Pc) was synthesized and purified according to a literature procedure.[37] The rare-earth trifluoroacetates were prepared by dissolving the respective rare-earth oxides in trifluoroacetic acid. All other chemicals were of analytical-reagent grade and used without further purification. The water used in all experiments was ultrapure.

Characterization

The size and morphologies of nanoparticles were determined at 300 kV using a TECNAI F-30 high-resolution transmission electron microscope. Energy-dispersive X-ray analysis (EDXA) of the samples was also performed during high-resolution TEM measurements. X-ray diffraction (XRD) measurements were recorded on a PANalytical X′pert PRO diffractometer using $Cu_{K\alpha}$ radiation, operating at 40 kV and 30 mA. UV/Vis absorption spectra were obtained with a DU-7400 UV/Vis spectrophotometer. The upconversion luminescence emission spectra were recorded on an USB 2000 VIS/NIR spectrometer (Ocean Optics), using an external 0–5 W adjustable 980 nm semiconductor laser (BWT Beijing Ltd) as the excitation source. Dynamic light scattering (DLS) and zeta-potential experiments were carried out on a Nano-ZS (Malvern Instruments).

Synthesis of $NaGdF_4$:Yb/Er/$NaGdF_4$ nanocrystals (UCNPs)

The UCNPs were synthesized according to a literature procedure with slight modifications.[30] Briefly, the $NaGdF_4$:Yb, Er core solution was prepared by mixing 1.25 mmol of $Re(CF_3COO)_3$ (Gd/Yb/Er = 78:20:2) and 1.25 mmol of sodium trifluoroacetate in 1-octadecene (2.5 mL) and oleic acid (5 mL, solution A). The $NaGdF_4$ shell solution was prepared by mixing 1.25 mmol of $Gd(CF_3COO)_3$ and 1.25 mmol of sodium trifluoroacetate in another reaction vessel with 1-octadecene (2.5 mL) and oleic acid (5 mL, solution B). Another mixture, which consisted of 1-octadecene (15 mL) and oleic acid (10 mL), was denoted as solution C. Solutions A, B, and C were degassed at 125 °C for 30 min under a gentle flow of argon to remove any residual water and oxygen. Subsequently, solution C was heated to 310 °C under an argon atmosphere and maintained at this temperature. Solution A (at 125 °C) was then added dropwise into solution C using a syringe pump (flow rate: 1.0 mL min^{-1}; KDS100, USA). After completing the addition, the reaction mixture was kept at 305 °C for 20 min under an argon atmosphere. Then, solution B (at 125 °C) was transferred dropwise into solution C at the same flow rate as for the addition of solution A. After completing the addition, the reaction mixture was kept at 305 °C for 20 min under an argon atmosphere with vigorous magnetic stirring. The solution was allowed to cool to room temperature. Nanocrystals were precipitated out by adding EtOH and were isolated via centrifugation (12 000 rpm, 6 min). The products were washed three times with cyclohexane/EtOH (1:8, v v^{-1}) to remove any impurities. The as-prepared nanocrystals could be easily re-dispersed in cyclohexane.

Preparation of UCNP@SiO_2(AlC_4Pc) Nanoparticles

To covalently bind the AlC_4Pc photosensitizer to the silica networks of the UCNP@SiO_2 nanoparticles, AlC_4Pc was first treated with APTES in the presence of EDC to form the AlC_4Pc silanization precursor. In a typical procedure, AlC_4Pc (420 μL, 4.8 mg mL^{-1} in DMSO) was mixed with APTES (20 μL). Next, EDC (12.8 mg) and NHS (8.8 mg) were added and the mixture was stirred for 24 h at room temperature. The obtained solution was directly used without further treatment. The UCNP@SiO_2(AlC_4Pc) nanoparticles were prepared by co-hydrolysis of the AlC_4Pc-functionalized silanization precursor with TEOS in a W/O microemulsion. In a typical procedure, Igepal CO-520 (0.35 mL), cyclohexane (4.5 mL), UCNPs cyclohexane solution (0.25 mL, 60.5 mg mL^{-1}), and ammonium hydroxide (0.035 mL, 29.4 %) were mixed in a vial (15 mL) to form a transparent microemulsion after sonication. Then, TEOS (40 μL) and the AlC_4Pc-functionalized silanization precursor (104 μL) were added and the reaction was continued for 50 h in the dark at room temperature. After that, the nanoparticles were isolated with EtOH, centrifuged, and washed with EtOH and water several times to remove any surfactant molecules and other unreacted materials.

The amount of Gd^{3+} ions in the UCNP@SiO_2(AlC_4Pc) nanoparticles was determined by the ICP-AES method: aqua regia and hydrofluoric acid were added to the UCNP@SiO_2(AlC_4Pc) nanoparticles and they were left overnight, then perchloric acid was added and the mixture was heated. After the solution was evaporated, the residue was dissolved and diluted in 5 % HNO_3 to determine Gd^{3+} content.

Singlet-Oxygen Detection

To assess the capability of UCNP@SiO_2(AlC_4Pc) nanoparticles for singlet-oxygen ($^1O_2$) generation, 1,3-diphenylisobenzofuran (DPBF) was used as a probe molecule.[33] DPBF reacts irreversibly with $^1O_2$ to cause a decrease in the DPBF absorption signal at 400 nm. In a typical experiment, DPBF (50 μL, 1.5 mg mL^{-1} in CH_3CN) was added to a solution of the nanoparticles in CH_3CN (2 mL, 1.5 mg mL^{-1}). Control experiments used DPBF with UCNP@SiO_2 nanoparticles and DPBF with free AlC_4Pc in CH_3CN. The solutions were then irradiated with a 980 nm laser source (2.19 A) for different time periods, and their optical densities at 400 nm were recorded in a DU-7400 spectrophotometer.

Cell Culture and Cellular Uptake

BNL 1ME A.7R.1 (MEAR), a mouse liver hepatoma cell-line, was purchased from the cell storeroom of the Chinese Academy of Science. Cells were grown in Dulbecco's modified Eagle's medium (DMEM) supplemented with 10% fetal bovine serum (FBS) and 5% CO_2 at 37°C. To test the uptake of UCNP@SiO_2(AlC_4Pc) nanoparticles, MEAR cells were plated in 35 mm tissue-culture dishes at a density of about 50000 cells per dish in DMEM. After incubation for 24 h, the culture medium was replaced by the same medium containing 100 μg mL^{-1} UCNP@SiO_2(AlC_4Pc) nanoparticles. After incubation for 12 h, the cells were washed three times with PBS and their nuclei were stained with 4′,6′-diamidino-2-phenylindole (DAPI) solution (5 μg mL^{-1}). Confocal fluorescence imaging was performed with an Olympus Fluoview 1000 laser-scanning microscope and a 60× oil-immersion objective lens. A He/Ne laser supplied the 633 nm excitation light to excite the nanoparticles, and a 650 nm long-pass filter was used to collect emission.

For the determination of Gd^{3+} ion uptake by the MEAR cells, after the UCNP@SiO_2(AlC_4Pc) nanoparticles were incubated with the cells for 24 h, the cells were washed and trypsined from the culture plate. The rest of the procedure was similar to that mentioned above, apart from that the sample was filtered through a 0.22 μm membrane after being dissolved in HNO_3.

Cytotoxicity of UCNP@SiO_2(AlC_4Pc) Nanoparticles

In vitro cytotoxicity was measured by a MTT assay. Briefly, MEAR cells were seeded in 96-well cell-culture plates (Nunc) at approximately $\times 10^4$ cells per well and incubated for 24 h at 37°C under a 5% CO_2 atmosphere. Various concentrations of UCNP@SiO_2(AlC_4Pc) nanoparticles (0, 10, 50, 100, 200, 300, and 500 μg mL^{-1}, diluted in DMEM) were then added to the wells. The cells were further incubated for 24 h at 37°C under a 5% CO_2 atmosphere. Subsequently, the MTT reagent (25 μL, 5 mg mL^{-1}) was added to each well and incubated for an additional 4 h at 37°C under a 5% CO_2 atmosphere. Then, the formazan product was dissolved in DMSO. After 10 min, the optical density at 490 nm (absorption value) of each well was measured on a Tecan Infinite M 200 monochromator-based multifunction microplate reader. Corresponding nanoparticles with cells that were not treated with MTT were used as a control. The cells vitality after labeling was compared with that of unlabeled cells and expressed as the relative ratio.

Photodynamic Effect of the Nanoparticles on MEAR Cells

For optical imaging to monitor the effect of PDT, MEAR cells were seeded in a 24-well plate at a density of $\times 10^5$ cells per well for 24 h. Then, the medium was replaced by a cell medium (0.5 mL per well) that contained 100 μg mL^{-1} of UCNP@SiO_2(AlC_4Pc) nanoparticles, UCNP@SiO_2 nanoparticles, or free AlC_4Pc. After incubation for 12 h, the cells were washed three times with PBS to remove the unbound nanoparticles. Then PBS (0.5 mL) was added and the cells were exposed to a 980 nm laser with a power density of 500 mW cm^{-2} for 2 and 5 min, respectively. After staining with trypan blue, optical imaging was performed by fluorescence microscopy.

In Vitro Relaxivities Measurements

Relaxivity data were determined on a Varian 7.0-T MR system from tubes that contained different concentrations of nanoparticles dispersed in water. Values of t_1 were obtained by fitting an increasing exponential function (saturation-recovery equation) to a signal-TR plot. Values of t_2 were obtained by fitting a decreasing monoexponential function to signal-TE plots. Values for r_1 and r_2 were calculated from the slope of linear regression fits of inverse relaxation times (relaxation rates) plotted against Gd^{3+} ion concentration. For t_1- and t_2-weighted MRI, the following parameters were adopted: 1) t_1, TR/TE = 100:15 ms, matrix = 128 × 128, FOV = 80 × 80, slice thickness = 2.0 mm; 2) t_2, TR/TE = 4000:50 ms, matrix = 128 × 128, FOV = 80 × 80, slice thickness = 2.0 mm. To observe the MR-contrast effect of the nanoparticles within the cells, after incubation of the nanoparticles with MEAR cells for 12 h, the adherent cells were detached from the plate by treatment with trypsin-EDTA and placed in a cell medium for MR imaging. Each tube contained approximately $\times 10^5$ cells.

Acknowledgements

This work was financially supported by the NSFC (21101131, 21021061, 20925103, and 20871100), by the Fok Ying Tung Education Foundation (121011), by an NSF of Fujian Province for Distinguished Young Investigator Grant (2009J06005), by the Fundamental Research Funds for the Central Universities (2010121015), by the Scientific Research Foundation for the Returned Overseas Chinese Scholars of State Education Ministry, and by the NFFTBS (J1030415). We thank Professor Donghui Li of the Cancer Centre of Xiamen University for the supply of AlC_4Pc, Dr. Jianli Zou in the University of Western Australia and Dr. Jing Yang for help with proofreading, and Dr. Qian Liu for help with the confocal images.

[1] W. M. Sharman, C. M. Allen, J. E. van Lier, *Drug Discovery Today* **1999**, *4*, 507–517.
[2] Y. N. Konan, R. Gruny, E. J. Allemann, *J. Photochem. Photobiol. B* **2002**, *66*, 89–106.
[3] D. E. J. G. J. Dolmans, D. Fukumura, R. K. Jain, *Nat. Rev. Cancer* **2003**, *3*, 380–387.
[4] S. B. Brown, E. A. Brown, I. Walker, *Lancet Oncol.* **2004**, *5*, 497–508.
[5] T. J. Dougherty, *Photochem. Photobiol.* **1987**, *45*, 879–899.
[6] R. Bonnett, *Chem. Soc. Rev.* **1995**, *24*, 19–33.
[7] T. J. Dougherty, *J. Clin. Laser Med. Surg.* **1996**, *14*, 219–221.
[8] J. D. Spikes in *Porphyrin Localization and Treatment of Tumors*, (Eds.: D. R. Doiron, C. J. Gomer), Alan R. Liss, New York, **1984**, pp. 19–39.
[9] D. Bechet, P. Couleaud, C. Frochot, M. L. Viriot, F. Guillemin, M. Barberi-Heyob, *Trends Biotechnol.* **2008**, *26*, 612–621.
[10] M. A. Oar, J. M. Serin, W. R. Dichtel, J. M. J. Frechet, T. Y. Ohulchanskyy, P. N. Prasad, *Chem. Mater.* **2005**, *17*, 2267–2275.
[11] A. Vogel, V. Venugopalan, *Chem. Rev.* **2003**, *103*, 577–644.
[12] C. F. van Nostrum, *Adv. Drug Deliv. Rev.* **2004**, *56*, 9–16.
[13] B. Chen, B. W. Pogue, T. Hasan, *Expert Opin. Drug Delivery* **2005**, *2*, 477–487.
[14] D. K. Chatterjee, L. S. Fong, Y. Zhang, *Adv. Drug Delivery Rev.* **2008**, *60*, 1627–1637.
[15] T. Y. Ohulchanskyy, I. Roy, L. N. Goswami, Y. H. Chen, E. J. Bergey, R. K. Pandey, A. R. Oseroff, P. N. Prasad, *Nano Lett.* **2007**, *7*, 2835–2842.
[16] X. X. He, X. Wu, K. M. Wang, B. H. Shi, L. Hai, *Biomaterials* **2009**, *30*, 5601–5609.
[17] Y. Cheng, A. C. Samia, J. D. Meyers, I. Panagopoulos, B. W. Fei, C. Burda, *J. Am. Chem. Soc.* **2008**, *130*, 10643–10647.
[18] R. R. Zhang, C. L. Wu, L. L. Tong, B. Tang, Q. H. Xu, *Langmuir* **2009**, *25*, 10153–10158.
[19] S. H. Cheng, C. H. Lee, C. S. Yang, F. G. Tseng, C. Y. Mou, L. W. Lo, *J. Mater. Chem.* **2009**, *19*, 1252–1257.
[20] F. Wang, X. L. Chen, Z. X. Zhao, S. H. Tang, X. Q. Huang, C. H. Lin, C. B. Cai, N. F. Zheng, *J. Mater. Chem.* **2011**, *21*, 11244–11252.

[21] J. Zhu, H. X. Wang, L. Liao, L. Z. Zhao, L. Zhou, M. H. Yu, Y. H. Wang, B. H. Liu, C. Z. Yu, *Chem. Asian J.* **2011**, *6*, 2332–2338.
[22] S. J. Lee, K. Park, Y. K. Oh, S. H. Kwon, S. Her, I. S. Kim, K. Choi, S. J. Lee, H. Kim, S. G. Lee, K. Kim, I. C. Kwon, *Biomaterials* **2009**, *30*, 2929–2939.
[23] P. Zhang, W. Steelant, M. Kumar, M. Scholfield, *J. Am. Chem. Soc.* **2007**, *129*, 4526–4527.
[24] D. K. Chatterjee, Y. Zhang, *Nanomedicine* **2008**, *3*, 73–82.
[25] H. S. Qian, H. C. Guo, P. C. L. Ho, R. Mahendran, Y. Zhang, *Small* **2009**, *5*, 2285–2290.
[26] J. N. Shan, S. J. Budijono, G. H. Hu, N. Yao, Y. B. Kang, Y. G. Ju, R. K. Prud′homme, *Adv. Funct. Mater.* **2011**, *21*, 2488–2495.
[27] C. Wang, H. Q. Tao, L. Cheng, Z. Liu, *Biomaterials* **2011**, *32*, 6145–6154.
[28] H. Vallhov, S. Gabrielsson, M. Stromme, A. Scheynius, A. E. Garcia Bennett, *Nano Lett.* **2007**, *7*, 3576–3582.
[29] F. Lu, S. H. Wu, Y. Hung, C. Y. Mou, *Small* **2009**, *5*, 1408–1413.
[30] Y. I. Park, J. H. Kim, K. T. Lee, K. S. Jeon, H. B. Na, J. H. Yu, H. M. Kim, N. Lee, S. H. Choi, S. I. Baik, H. Kim, S. P. Park, B. J. Park, Y. W. Kim, S. H. Lee, S. Y. Yoon, I. C. Song, W. K. Moon, Y. D. Suh, T. Hyeon, *Adv. Mater.* **2009**, *21*, 4467–4471.
[31] J. C. Boyer, J. Gagnon, L. A. Cuccia, J. A. Capobianco, *Chem. Mater.* **2007**, *19*, 3358–3360.
[32] H. A. Collins, M. Khurana, E. H. Moriyama, A. Mariampillai, E. Dahlstedt, M. Balaz, M. K. Kuimova, M. Drobizhev, V. X. D. Yang, D. Phillips, A. Rebane, B. C. Wilson, H. L. Anderson, *Nat. Photonics* **2008**, *2*, 420–424.
[33] W. Spiller, H. Kliesch, D. Wohrele, S. Hackbarth, B. Roder, G. J. Schnurpfeil, *J. Porphyrins Phthalocyanines* **1998**, *2*, 145–158.
[34] C. Cantau, T. Pigot, N. Manoj, E. Oliveros, S. Lacombe, *ChemPhysChem* **2007**, *8*, 2344–2353.
[35] H. Guo, Z. Q. Li, H. S. Qian, Y. Hu, I. N. Muhammad, *Nanotechnology* **2010**, *21*, 125602.
[36] R. Kumar, M. Nyk, T. Y. Ohulchanskyy, C. A. Flask, P. N. Prasad, *Adv. Funct. Mater.* **2009**, *19*, 853–859.
[37] F. P. Chen, D. Y. Xu, *Chin. J. Org. Chem.* **1990**, *10*, 550–553.

Received: October 25, 2011
Published online: January 25, 2012

